Proceedings of ISFOG 2025
5TH INTERNATIONAL SYMPOSIUM ON
FRONTIERS IN OFFSHORE GEOTECHNICS
Nantes, France | June 9-13 2025
© 2025 the Authors
ISBN 978-2-85782-758-0

Towards efficient end-of-life solutions in offshore wind

X. Yin
AtkinsRéalis, London, UK; formerly Imperial College London, UK
K. Vinck*, L. Zdravković
Imperial College London, London, UK
**ken.vinck15@imperial.ac.uk*

ABSTRACT: Offshore wind farms, facilitating the exploitation of wind power as a renewable energy source, have grown rapidly in many parts of the world, including the North Sea, over the past decade. Their design life is envisaged to be approximately 25 years, and the current default end-of-life solution is that of full decommissioning, whereby developers are expected to remove all parts of the wind farm and restore the seabed to its prior condition. However, as some of the oldest installations are now nearing the end of their life, different forms of life extension for existing sites are considered as alternative and more sustainable solutions compared to full decommissioning. Some current studies consider partial decommissioning of a wind turbine, which involves completely removing the superstructure to the seabed level, leaving the original monopile embedded in the seabed. Considering that the power and size of turbines have been increasing, a new turbine will most likely need the support of a larger monopile, which could be installed to enclose the existing smaller monopile. The potential benefit of this approach is the avoidance of seabed disturbance by prior extraction of the existing monopile and the associated costs of such extraction. The study in this paper is exploratory and numerical in nature, utilising finite element analysis and parametric variations of monopile geometries in two distinctive seabed settings: a glacial till and a dense marine sand. The results focus on identifying the interaction mechanisms between the two monopiles based on their geometry.

Keywords: Monopile, Pile-over-pile, End-of-Life, Decommissioning, Finite Element Analysis

1 INTRODUCTION

Since the first commissioning projects in 1991, the offshore wind industry has made significant advances over the past decades. Looking forward, the Global Wind Energy Council (GWEC) projects that global offshore wind capacity will increase to 380 GW by 2030 and 2,000 GW by 2050, making offshore wind a cornerstone of the global transition to renewable energy (GWEC, 2024).

Monopile foundations are the most commonly used foundation type in the offshore wind industry, particularly in the European North Sea and Baltic Sea sectors. These large cylindrical steel structures support a majority of offshore wind turbines due to their cost-effectiveness, simplicity in design, and ease of installation.

As the offshore wind industry continues to expand, many of the first-generation wind farms are approaching the end of their operational lives (EoL). Monopiles installed in the early 2000s, with an expected lifespan of 25 years, are now facing an EoL scenario. It is estimated that by 2030, around 600 offshore wind turbines will reach their EoL, with 72% of these structures being monopile-supported (Spyroudi, 2021). The current strategies for dealing with offshore wind turbine EoL scenarios include:

- *Lifetime extension* involves keeping turbines operational beyond their 25-year design life with minor repairs.
- *Repowering* involves upgrading or replacing turbines while potentially retaining existing foundations.
- *Decommissioning* is the most common strategy currently applied as a default solution, where turbines and foundations are fully extracted, or partially removed from/above the seabed level.

Several challenges are currently identified in decommissioning methodologies. These include financial and environmental risks from existing monopile cutting techniques, including both internal and external cutting, a lack of clear regulations tailored to offshore wind, and limited availability of specialised vessels, which increase the costs of decommissioning monopiles (Topham et al, 2019). The impact on marine ecosystems is another concern, particularly when deciding between full or partial removal of foundations. Additionally, underwater hazards may arise if monopile remains become exposed due to tidal movements.

Offshore wind turbine monopiles are primarily designed to resist lateral loads from winds and waves. Cyclic loading causes fatigue in both the monopile and surrounding soil, impacting structural integrity and foundation stiffness. Fatigue and bending can lead to deterioration of steel at critical points, posing stability risks.

Given the challenges associated with traditional decommissioning strategies, this study explores a novel approach of a Pile-over-Pile (PoP) system, which involves removal of the upper components of a wind turbine above the seabed level (including the turbine itself and the support tower down to the seabed level), the embedded part of an existing monopile remaining in the seabed. A new bigger monopile is then installed over the existing monopile, thereby reusing the old pile while avoiding the disturbance of the seabed that would be caused by its removal. It is emphasised that the study primarily consideres geometric interactions between wished-in-place monopiles, ignoring the effects of possible long-term stress changes in the seabed around the existing monopile, or those induced by the installation of a new monopile.

2 METHODOLOGY

2.1 Pile-over-Pile overview

With reference to Figure 1, the contour of the red line represents the original inner monopile, characterised by its geometric properties: diameter D, embedded length L, and the eccentricity of the horizontal load application h above the seabed level. The respective geometric properties of the new outer monopile, installed over the inner monopile, are denoted as D_1, L_1 and h_1.

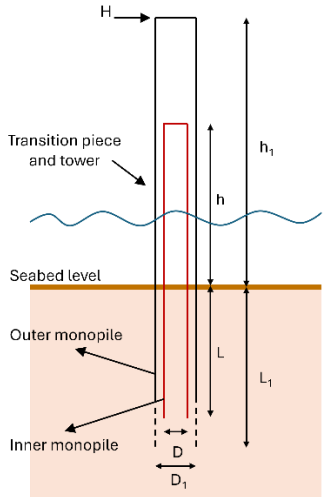

Figure 1.Geometry for Pile-over-pile system

2.2 Initial Ground Conditions

The study adopts two distinct ground conditions characterised by the PISA (Pile Soil Analysis) project (Zdravković et al., 2020a), which are considered representative of certain sectors of the North Sea. These include a dense marine sand site at Dunkirk, France, and a stiff low-plasticity clay till site at Cowden, UK.

The initial ground profile at Dunkirk comprises natural sand with the initial relative density, D_R, void ratio, e_0, saturated bulk unit weight, γ, and the earth pressure coefficient at rest, K_0, as summarised in Table 1. The pore pressure is hydrostatic with depth.

Table 1. Summary of initial parameters for Dunkirk site.

D_R [%]	e_0	K_0	γ [kN/m^3]
75%	0.629	0.4	19.9

The initial ground conditions at Cowden are characterised by the saturated bulk unit weight $\gamma = 21.19\ \mathrm{kN/m^3}$ and the K_0 and OCR (over-consolidation ratio) profiles which reduce with depth, to reflect the interpreted profile of the undrained shear strength, S_u, as discussed in Zdravković et al., 2020a and Byrne et al. (2020). The pore water pressure profile is hydrostatic with depth.

2.3 Constitutive Modelling

The constitutive model for Dunkirk sand is a state parameter-based bounding surface plasticity model, as detailed in Taborda et al. (2014). This model is capable of capturing the effects of void ratio, e, and mean effective stress, p', changes on the behaviour of sands. The model calibration is derived from the PISA site and soil characterisation, as described in Taborda et al. (2020).

The constitutive model for Cowden clay is a generalised and extended version of the modified Cam clay model (Roscoe and Burland, 1968). Key extensions include a nonlinear small-strain stiffness overlay (Taborda and Zdravković, 2014) to capture the dependency of shear and bulk stiffness on stress and strain levels; a Hvorslev surface (Potts and Zdravković, 1999) to provide a more accurate representation of the undrained shear strength of overconsolidated clays; and the Van Eekelen (1980) expression to account for a realistic variation of soil strength in the deviatoric plane. The derivation of model parameters is based on PISA laboratory and field data, as detailed in Zdravković et al. (2020b).

For brevity, the derived parameters for both constitutive models are not summarised in this paper but are available in the references cited above.

2.4 Numerical Model

All analyses reported in this study are conducted using the Imperial College Finite Element Program, ICFEP (Potts and Zdravković, 1999). The 3D finite element (FE) mesh shown in Figure 2 utilises the plane of symmetry in the problem of a laterally loaded pile, allowing only half of the problem to be discretised.

The soil in the numerical model (Dunkirk sand or Cowden clay) is discretised using 20-noded hexahedral elements, each with three displacement degrees of freedom per node. The domain, extending 100 m in depth and 100 m radially from the vertical monopile axis, is sufficiently large to eliminate any boundary effects that might influence the analysis results.

The steel open-ended tubular monopiles in the FE mesh are discretised using 8-noded shell elements (Schroeder et al., 2007), with three displacement and three rotational degrees of freedom per node. The monopiles are assumed as linear elastic, with a Young's modulus of 200 GPa and a Poisson's ratio of 0.3.

The outer monopile-soil interface is discretised using 16-noded zero-thickness interface elements (Day and Potts, 1994). These are modelled as linear elastic-plastic, with normal and shear elastic stiffness values of $K_N = K_S = 1.0 \times 10^5$ kN/m^3, and a limited tensile capacity (assumed to be zero). This modelling approach allows a gap to open around a laterally loaded monopile when the normal effective interface stress reduces to zero.

The bottom boundary of the mesh is fully constrained in all three coordinate directions. The cylindrical vertical boundary is constrained perpendicular to the boundary, as is the vertical plane of symmetry. The relevant rotational degrees of freedom along the edges of monopile shell elements are also constrained. Monopile loading is simulated with the application of incremental uniform horizontal displacements (parallel to the plane of symmetry) at the top of the tower, with the load determined as a reaction to the applied displacements.

The inset in Figure 2 illustrates the analysed PoP configuration of embedded monopiles. In the PoP setup, the tower of the inner monopile is removed from the mesh. The analyses are performed as drained for monopiles in Dunkirk sand and undrained for monopiles in Cowden clay. The mobilised limit load is assumed to be reached when the horizontal ground surface displacement on the passive side of the outer monopile reaches 10% of the pile diameter.

Table 2 summarises the combinations of monopile geometries selected to examine the extent of PoP interactions. The dimensions of the inner monopiles are part of the geometric parameter space investigated in the PISA project, which also included monopiles with a 10 m diameter.

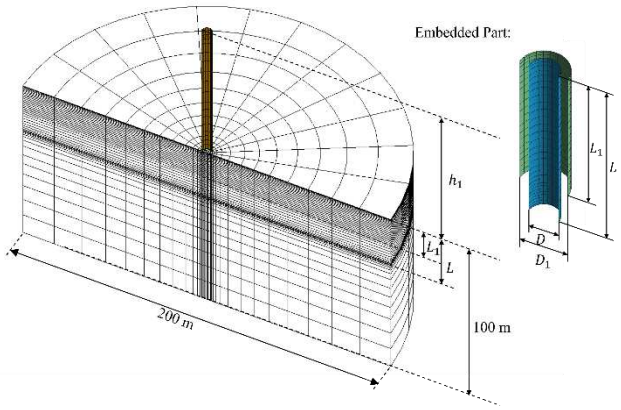

Figure 2. Example FE mesh of Pile-over-Pile analysis

Table 2.Summary of pile geometries analysed in the study for Dunkirk Sand (D) and Cowden Till (C)

	Inner Monopile							**Outer Monopile**					
	h/D	**L/D**	**D/t**	**D[m]**	**L[m]**	**h[m]**	**t[mm]**	**L_1/ D_1**	**D_1/ t_1**	**D_1 [m]**	**L_1 [m]**	**h_1 [m]**	**t_1 [mm]**
D1, C1	5	2	110	5	10	25	45	2	100	5.5	11	27.5	55
D2, C2	5	2	110	5	10	25	45	2	100	8	16	40	80
D3	15	6	110	5	30	75	45	3	100	10	30	150	100
D4	15	6	110	5	30	75	45	3	100	5.5	16.5	82.5	55
D5, C7	15	6	110	5	30	75	45	3	100	8	24	120	80
D6	15	6	110	5	30	75	45	3	100	9	27	135	90
D7, C4	15	4	110	7.5	30	112.5	68	2	100	9	18	135	90
D8, C5	15	4	110	7.5	30	112.5	68	3	100	9	27	135	90
D9, C3	15	4	110	7.5	30	112.5	68	4	100	9	36	135	90
C6	15	6	110	5	30	75	45	3	100	6	18	90	60
C8	15	6	110	5	30	75	45	2.67	100	9	24	135	90
C9	15	6	110	5	30	75	45	2.40	10	10	24	250	100

3 RESULTS AND DISCUSSION

3.1 Load-displacement response

Analyses D1, D2, and C1, C2 represent two example cases where the inner monopile is entirely enclosed by the new outer monopile. A $D = 5$ m and $L = 10$ m inner monopile ($L/D = 2$) is enclosed by an outer monopile with an increasing diameter, ranging from 10% to 80% larger than the diameter of the inner monopile, while maintaining the same L_1/D_1 and h_1/D_1 ratios of the inner pile. The thickness of the outer monopile is determined using a diameter-to-thickness ratio, D_1/t_1, that is kept constant at 100. Since the outer monopile in both cases is longer than the inner monopile, the resulting load-displacement curves are only marginally influenced by the presence of the inner monopile. This prediction holds true for both Dunkirk and Cowden ground conditions. These curves are not included for brevity.

The interaction effects become apparent when the new outer monopile is shorter than the existing monopile. A set of results is presented in Figure 3 for analyses D3 to D6. A $D = 5$ m and $L = 30$ m inner monopile ($L/D = 6$) is overlaid by an outer monopile with an increasing diameter but a constant $L_1/D_1 = 3$. While maintaining the same h_1/D_1 ratio of 15, the embedded length of the outer monopile increases from nearly 50% of the inner monopile length ($L_1 = 16.5$ m, analysis D4) to being equal to the inner monopile length ($L_1 = 30$ m, analysis D3).

The graphs of the horizontal force, H, at the top of the outer monopile tower, against the horizontal displacement, u, at the seabed level on the passive side of the monopile, clearly demonstrate the extent of the contribution made by the existing inner monopile to the capacity of the PoP system. Although both D_1 and L_1 are changing, the results suggest that the length of the outer monopile dominates the pile interaction.

For the case of the shortest outer monopile (analysis D4), a nearly 100% capacity increase in the PoP system capacity is predicted. However, this additional capacity reduces as the length of the outer pile increases and completely diminishes when the outer monopile length equals that of the inner monopile (analysis D3), at which point the inner monopile is entirely enclosed by the outer monopile.

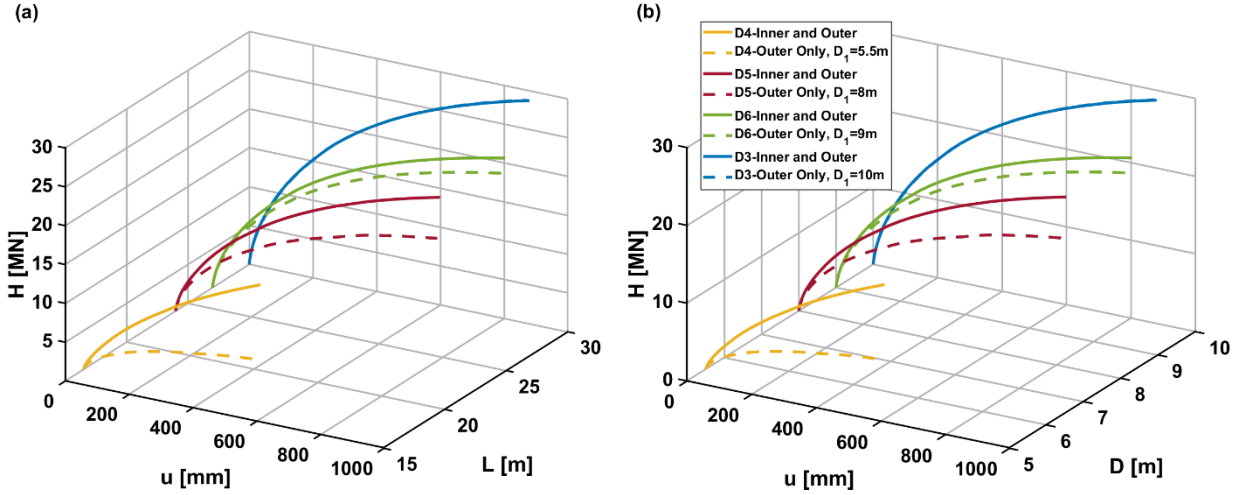

Figure 3. Load-displacement curves for analyses D3 to D6, Inner monopile base geometry $D = 5m$, $L/D = 6$, Outer monopile $L_1/D_1 = 3$, $h_1/D_1 = 15$: (a) Increasing the length and (b) increasing the diameter of the outer monopile.

As the relative results from the analyses with either of the two ground conditions are similar, Figure 4 presents the load-displacement curves for the Cowden ground conditions (analyses C3 to C5), where the diameter of the outer monopile is fixed at $D_1 = 9$ m (20% larger than the $D = 7.5$ m of the inner pile), while the L_1/D_1 ratio, and consequently the length, increases.

These results isolate the effect of the outer pile diameter and once again demonstrate the dominant influence of the outer pile length, as seen in Figure 3. The PoP system's capacity is primarly enhanced by the presence of the inner monopile in the case of the shortest outer monopile (C4) and diminishes when the inner pile is fully enclosed by the outer pile (C5).

In a similar manner, Figure 5 presents the results of analyses C7 to C9, where the length of the outer monopile is kept constant at $L_1 = 24$ m, while D_1 increases as the L_1/D_1 ratio decreases. While the capacity of both the outer monopile alone and the PoP system increases with the outer monopile diameter, its effect on the interaction between the two monopiles is significantly smaller than that of the monopile length.

The enhanced capacity of the PoP system is reduced only slightly for the examined geometries.

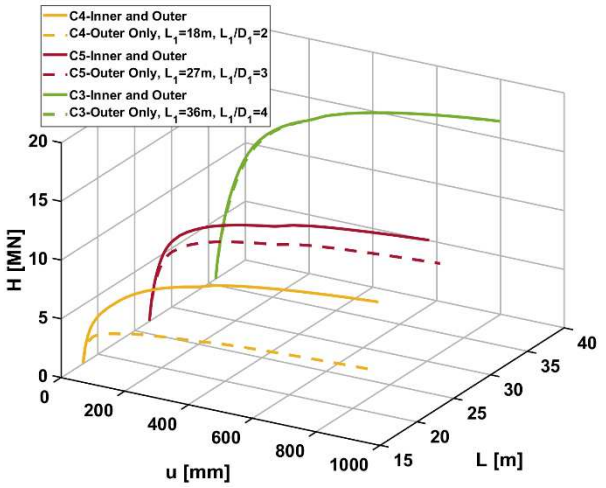

Figure 4. Load-displacement curves for analyses C3 to C5: Increasing L_1 with $D_1 = 9m$; inner monopile base geometry $D = 7.5\ m$, $L/D = 4$.

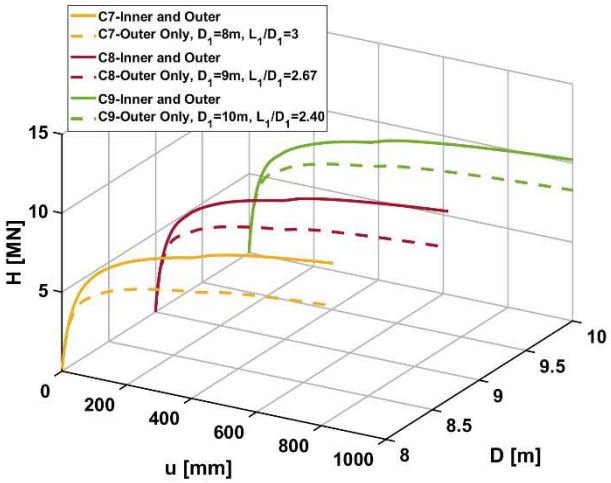

Figure 5. Load-displacement curves for analyses C7 to C9: Increasing D_1 with $L_1 = 24m$; inner monopile base geometry $D = 5\ m$, $L/D = 6$.

3.2 Deflection and Bending Moment Profiles

As shown in the load-displacement response for analyses D1 to D3 and C1 and C2, where the inner monopile is fully enclosed by the outer monopile, the overall PoP system deflection is not influenced by the presence of the inner monopile.

The existing inner monopile begins to affect the PoP system deflection when the outer monopile is shorter and less flexible. Figure 6 presents deflection profiles with normalised horizontal displacement and pile length for both PoP and outer-only scenarios when the horizontal ground displacement reaches nominal ultimate conditions ($0.1D$ & $0.1D_1$) in analyses D7 to D9. The inner monopile base geometry is $D = 7.5$ m and $L = 30$ m, while the outer monopile ($D_1 = 9$ m) varies its embedded length with L_1/D_1 from 2 to 4.

In the D9 analysis, the inner monopile is fully enclosed by the outer monopile, and the PoP deflection profile coincides with that of the inner monopile alone. As the outer monopile shortens, the PoP interaction shifts the centre of rotation downwards, reaching its extreme (base rotation) in the D7 analysis, where L_1 is nearly half of L. Figure 6 illustrates the interaction effects by comparing the deflection profiles of the PoP system (a) with those of the outer-only scenario (b).

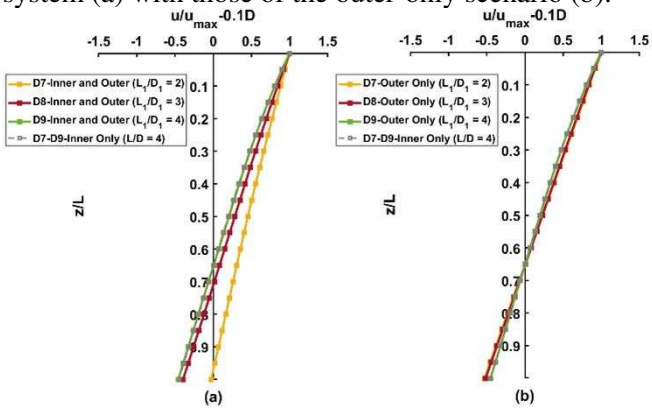

Figure 6. Normalised deflection curves of analyses D7 to D9, with $L/D = 4$ and $L_1/D_1 = 2, 3, 4$

To assess the inner monopile's contribution to system stiffness, deflection and distributed bending moment results along the embedded length were extracted. Figures 7 and 8 show findings from analyses D5 and D9 (analogous clay cases C3 and C7 not shown), comparing behaviour at larger ($0.1D$, Figure 7) and smaller displacement levels ($0.001D$, Figure 8). Both sand and clay profiles exhibit similar patterns.

In analysis D5 (C7), the shorter outer monopile has a diameter (D_1) increased by 60% relative to D. Conversely, in analysis D9 (C3), the longer outer monopile fully encloses the inner monopile, with D_1 increased by only 20% relative to D.

From Figures 7 and 8, the results for analysis D5 show that the PoP system has a greater bending moment capacity (Fig. 7b and 8b) and smaller deflection (Fig. 7a) compared to the standalone outer monopile. At small displacements, the real pile deflection (Fig. 8a) maintains a consistent shape, indicating minimal interaction effects between the two piles under these conditions.

Returning to the fully enclosed analysis D9, the interaction between the two piles is still evident (Fig. 7b), as the bending moment along the mid-embedded length of the pile is higher, despite the minimal interaction observed in the load-displacement and deflection. In contrast, when the outer monopile diameter increases substantially (Analysis D3, with a 100% increase in D), the large distance between the two piles reduces the degree of interaction and its associated stiffness contribution.

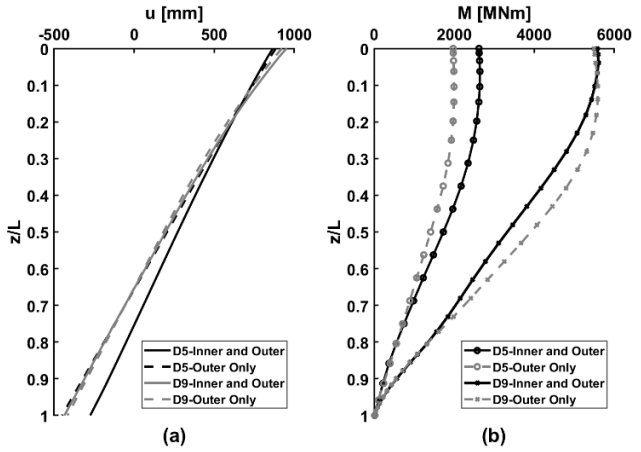

Figure 7.(a)Deflection and (b) Bending moment diagram of analysis D5, D9 in ultimate displacement level.

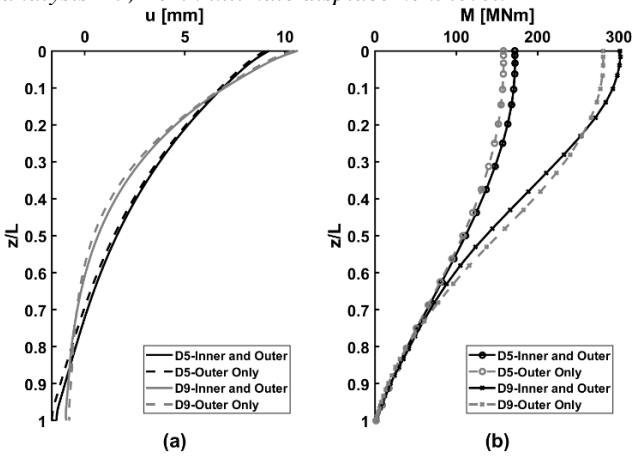

Figure 8.(a)Deflection and (b) Bending moment diagram of analysis D5, D9 in small displacement level.

4 CONCLUSION

This study systematically evaluates the interaction between an existing monopile left in the seabed and a new outer monopile to form a PoP system. It examines how geometric configurations affect load-displacement responses, deflection patterns, and bending moment distributions. The following key conclusions can be drawn:

a) Limited interaction in a fully enclosed PoP system, only bending moment contribution when pile walls are close.
b) The existing monopile enhances the capacity of the system when the outer monopile is shorter, while the length of the outer monopile has a more dominant effect than its diameter.
c) Inner monopile relative length and flexibility influence the flexibility of the PoP system.
d) Interaction mechanisms of the PoP system were similar in both ground conditions, indicating marginal sensitivity to conventional soil types.

AUTHOR CONTRIBUTION STATEMENT

X. Yin: Formal analysis, Results interpretation, Writing- Original draft. **K. Vinck**: Concept, Supervision, Writing- Reviewing and Editing. **L. Zdravković**: Software, Methodology, Supervision, Writing- Reviewing and Editing.

REFERENCES

Byrne, B. W. et al. (2020) PISA design model for monopiles for offshore wind turbines: application to a stiff glacial clay till, Géotechnique, 70(11), pp. 1030–1047. https://doi.org/10.1680/jgeot.18.P.255

Day, R. A. & Potts, D. M. (1994) Zero thickness interface elements – numerical stability and application, Int. J. for Numerical and Analytical Methods in Geomechanics, 18(10), pp. 689–708. https://doi.org/10.1002/nag.1610040107

GWEC. (2024) Global Offshore Wind Report 2024, GWEC.

Potts, D. M. & Zdravković, L. (1999) Finite element analysis in geotechnical engineering, Thomas Telford.

Roscoe, K. H. & Burland, J. B. (1968) On the generalized stress–strain behaviour of wet clay. In: Engineering Plasticity (eds J. Heyman & F. A. Leckie), pp. 535–609. Cambridge University Press, Cambridge, UK.

Schroeder, F. C. et al. (2007) Quadrilateral isoparametric shear deformable shell element for use in soil–structure interaction problems, Int. J. of Geomechanics, 7(1), pp. 44–52.

Spyroudi, A. (2021) End-of-life planning in offshore wind, ORE Catapult.

Taborda, D. M. G. et al. (2014) Computational study on the modification of a bounding surface plasticity model for sands. Elsevier BV.

Taborda, D. M. G. et al. (2020) Finite-element modelling of laterally loaded piles in a dense marine sand at Dunkirk, Géotechnique, 70(11), pp. 1014–1029. https://doi.org/10.1680/jgeot.18.PISA.006

Topham, E. et al. (2019) Challenges of decommissioning offshore wind farms: Overview of the European experience, J. of Physics: Conference Series, 1222(1), 012035. https://doi.org/10.1088/1742-6596/1222/1/012035

Van Eekelen, H. A. M. (1980) Isotropic yield surfaces in three dimensions for use in soil mechanics, Int. J. for Numerical and Analytical Methods in Geomechanics, 4(1). https://doi.org/10.1002/nag.1610040107

Zdravković, L. et al. (2020a) Ground characterisation for PISA pile testing and analysis, Géotechnique,

70(11), pp. 945–960. https://doi.org/10.1680/jgeot.18.PISA.001

Zdravković, L. et al. (2020b) Finite-element modelling of laterally loaded piles in a stiff glacial clay till at Cowden, Géotechnique, 70(11), pp. 999–1013. https://doi.org/10.1680/jgeot.18.PISA.005

INTERNATIONAL SOCIETY FOR
SOIL MECHANICS AND
GEOTECHNICAL ENGINEERING

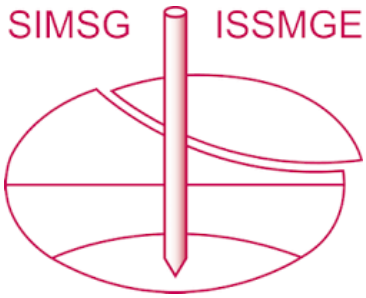

This paper was downloaded from the Online Library of the International Society for Soil Mechanics and Geotechnical Engineering (ISSMGE). The library is available here:

https://www.issmge.org/publications/online-library

This is an open-access database that archives thousands of papers published under the Auspices of the ISSMGE and maintained by the Innovation and Development Committee of ISSMGE.

The paper was published in the proceedings of the 5th International Symposium on Frontiers in Offshore Geotechnics (ISFOG2025) and was edited by Christelle Abadie, Zheng Li, Matthieu Blanc and Luc Thorel. The conference was held from June 9th to June 13th 2025 in Nantes, France.